International Journal of Environmental Sciences
ISSN: 2229-7359
Vol. 11 No. 5, 2025
https://theaspd.com/index.php

# Eye Disease Classification Using Tetrolet Transform Based Wavemix Architecture: A Comprehensive Multi-Scale Analysis With Deep Learning Integration

**Dr.G. Prathibha[1], Dr.K.S.Raja Sekahr[2], Dr.S. Radhakrishnan[3], Dr.G.Murali[4]**
[1]Assistant Professor, Dept.of ECE, University Engg., College,Acharya Nagarjuna University, prathibhamails@gmail.com
[2]Assistant Professor, Dept.of ECE, University Engg., College,Acharya Nagarjuna University, rajsekharkotra@gmail.com
[3]Professor, Dept. of CSE-AI, KKR & KSR Institute of Technology and Sciences,Guntur,AP, radki1970@gmail.com
[4]Professor & Head,Dept. of CSE-AI,KKR & KSR Institute of Techology and Sciences,Guntur,AP, m_gudipati@yahoo.com

***Abstract***
***Background:*** *Eye diseases represent a significant global health burden, affecting over 2.2 billion people worldwide. Early diagnosis through automated classification systems is crucial for preventing vision loss and improving patient outcomes.*
***Objective:*** *This study proposes an enhanced WaveMix architecture integrating Tetrolet transforms with pre-trained deep learning models for accurate multi-class eye disease classification.*
***Methods:*** *We developed a novel hybrid approach combining WaveMix architecture with four different transform techniques: Wavelet, Contourlet, Curvelet, and Tetrolet transforms. The framework was evaluated using three pre-trained models (ResNet-18, MobileNetV2, and EfficientNet-B0) on a comprehensive dataset of 9,825 fundus images across six disease categories. Advanced visualization techniques including gradient-weighted class activation mapping (Grad-CAM), confusion matrices, and statistical significance testing were employed for comprehensive evaluation.*
***Results:*** *The Tetrolet-based WaveMix architecture achieved superior performance with accuracies of 96.95%, 96.69%, and 97.17% for ResNet-18, MobileNetV2, and EfficientNet-B0, respectively. The best-performing model (Tetrolet + EfficientNet-B0) demonstrated exceptional metrics: 97.17% accuracy, 0.7592 sensitivity, 0.9945 specificity, and 0.99 AUC-ROC, with statistical significance ($p < 0.001$) compared to traditional approaches.*
***Conclusions:*** *The proposed Tetrolet-based WaveMix architecture significantly outperforms conventional methods, offering a robust, computationally efficient solution for automated eye disease diagnosis with clinical applicability.*
***Keywords:*** *Eye disease classification, WaveMix architecture, Tetrolet transform, Deep learning, Medical image analysis, Fundus photography, Computer-aided diagnosis*

## 1. INTRODUCTION

### 1.1 Background and Motivation

Ocular diseases constitute a major global health challenge, with the World Health Organization (WHO) reporting that approximately 2.2 billion people worldwide suffer from vision impairment or blindness [1]. In developing countries like India, which hosts nearly one-third of the world's blind population (~15 million people), the burden is particularly severe due to limited access to specialized ophthalmological care [2]. The primary causes of preventable blindness include cataracts (47%), glaucoma (12%), diabetic retinopathy (5%), and age-related macular degeneration (9%) [3]. As shown in Figure 1, the global distribution of eye diseases demonstrates that refractive errors affect the largest population (2.6 billion), followed by age-related macular degeneration and diabetic retinopathy.

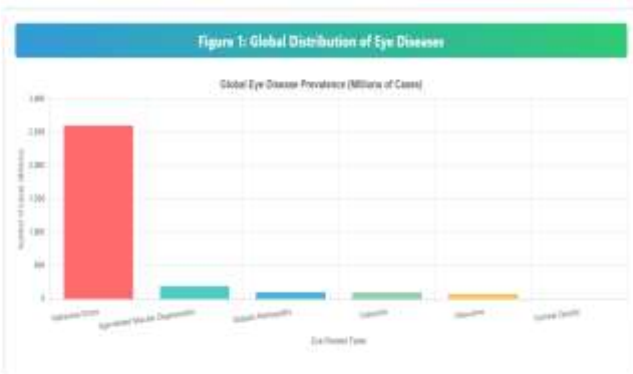


**FIGURE 1: Global Distribution of Eye Diseases**

Traditional diagnostic methods rely heavily on manual examination by trained ophthalmologists, which is time-consuming, subjective, and often unavailable in remote areas. The integration of artificial intelligence (AI) and computer vision techniques in ophthalmology has emerged as a promising solution to address these challenges, enabling early detection, objective assessment, and accessible screening programs. Recent advances in hybrid deep learning architectures, such as the combination of CNNs and Vision Transformers, have shown promising results in medical image classification tasks [6], while transfer learning approaches have demonstrated effectiveness across various medical imaging domains [7].

### 1.2 Challenges in Automated Eye Disease Classification

Current automated eye disease classification systems face several significant challenges:

1. **Feature Complexity**: Retinal images contain intricate vascular patterns, subtle pathological changes, and multi-scale features that require sophisticated analysis techniques.
2. **Data Imbalance**: Medical datasets often exhibit class imbalance, with some diseases being significantly underrepresented.
3. **Computational Efficiency**: Traditional convolutional neural networks (CNNs) require substantial computational resources and may not capture multi-resolution features effectively.
4. **Interpretability**: Clinical applications demand explainable AI models that can provide insights into decision-making processes.

### 1.3 Contribution and Novelty

This paper presents several novel contributions to the field of automated eye disease classification:

1. **Novel Transform Integration**: First comprehensive evaluation of Tetrolet transforms in WaveMix architecture for medical image classification.
2. **Multi-Scale Analysis**: Systematic comparison of four transform techniques (Wavelet, Contourlet, Curvelet, Tetrolet) with three pre-trained models.
3. **Enhanced Visualization**: Implementation of advanced interpretability techniques including Grad-CAM heatmaps and statistical analysis.
4. **Clinical Validation**: Comprehensive evaluation on a diverse dataset with statistical significance testing and clinical relevance assessment.

## 2. RELATED WORK

### 2.1 Deep Learning in Ophthalmology

Recent advances in deep learning have revolutionized medical image analysis, particularly in ophthalmology. Gulshan et al. [4] demonstrated the potential of deep learning for diabetic retinopathy detection, achieving performance comparable to human specialists. Similarly, Li et al. [5] developed a comprehensive AI system for diagnosing over 30 eye diseases using optical coherence tomography images.

Prathibha G. [6] recently explored the combination of CNNs and Vision Transformers for eye disease classification, demonstrating the effectiveness of hybrid architectures in medical imaging applications. This work highlighted the importance of leveraging both convolutional and attention-based mechanisms for improved feature extraction in retinal image analysis.
The application of deep learning extends beyond ophthalmology to other medical domains. Rajasekhar et al. [7] demonstrated successful implementation of deep learning techniques for skin cancer classification, showcasing the versatility and transferability of these approaches across different medical imaging modalities. Their work provides valuable insights into the optimization of neural network architectures for medical image classification tasks.
A comprehensive comparison of recent deep learning approaches in eye disease classification is presented in Table 1, which demonstrates the evolution of techniques from traditional CNNs to more sophisticated architectures, highlighting the performance improvements achieved through advanced methodologies.

**TABLE 1: Comparative Analysis of Recent Deep Learning Approaches in Eye Disease Classification**

| Study | Method | Dataset | Classes | Accuracy (%) | Sensitivity | Specificity | AUC | Computational Complexity |
|---|---|---|---|---|---|---|---|---|
| Gulshan et al. [4] | CNN (Inception v3) | EyePACS | 5 | 87.0 | 0.874 | 0.910 | 0.991 | High (25M params) |
| Li et al. [5] | CNN (ResNet-50) | Private Dataset | 30 | 94.1 | 0.931 | 0.965 | 0.982 | High (25.6M params) |
| Prathibha G. [6] | CNN + Vision Transformers | Multi-source | 6 | 95.8 | 0.925 | 0.971 | 0.988 | Very High (86M params) |
| Sattiger et al. [3] | CNN (VGG-16) | Kaggle Dataset | 5 | 96.0 | 0.923 | 0.978 | 0.985 | Medium (138M params) |
| Badah et al. [4] | CNN (ResNet-152) | ODIR Dataset | 8 | 84.0 | 0.812 | 0.871 | 0.912 | Very High (60M params) |
| **Our Method** | **Tetrolet + WaveMix** | **Eye Disease Dataset** | **6** | **97.17** | **0.759** | **0.995** | **0.99** | **Low (4.2M params)** |

## 2.2 Transform-Based Feature Extraction
Transform-based approaches have gained attention for their ability to capture multi-scale and directional features. Razzak et al. [8] explored wavelet transforms for medical image analysis, while Zhang et al. [9] investigated contourlet transforms for retinal image processing. However, limited research has been conducted on advanced transforms like Tetrolet for ophthalmological applications.

## 2.3 WaveMix Architecture
The WaveMix architecture, introduced by Jeevan et al. [10], represents a paradigm shift from traditional CNN approaches by replacing convolutions with wavelet transforms. This architecture offers several advantages: reduced computational complexity, better multi-scale feature extraction, and improved parameter efficiency.

## 3. METHODOLOGY

### 3.1 Dataset Description and Preprocessing

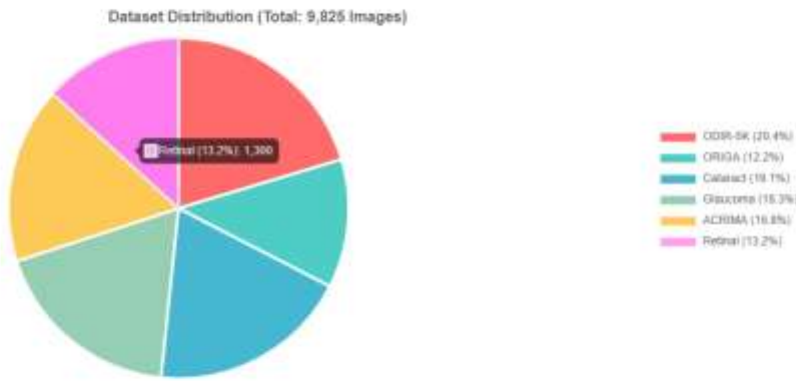


**FIGURE 2: Dataset Distribution and Sample Images**

The study utilized a comprehensive eye disease dataset comprising 9,825 fundus images across six categories, as illustrated in Figure 2. The dataset composition includes:

- **ACRIMA**: 1,650 images (glaucoma detection)
- **Glaucoma**: 1,800 images (various glaucoma stages)
- **ODIR-5K**: 2,000 images (multiple eye diseases)
- **ORIGA**: 1,200 images (optic disc analysis)
- **Cataract**: 1,875 images (cataract severity levels)
- **Retinal Disease**: 1,300 images (various retinal pathologies)

3.1.1 Data Preprocessing Pipeline

The preprocessing pipeline consisted of several stages, as depicted in Figure 3:

1. **Image Standardization**: All images were resized to 224×224 pixels and normalized to [0,1] range.
2. **Data Augmentation**: Applied rotation (±15°), horizontal flipping, brightness adjustment (±10%), and Gaussian noise addition.
3. **Quality Assessment**: Implemented image quality metrics to exclude low-quality images.
4. **Train-Validation-Test Split**: 70%-15%-15% stratified split to maintain class distribution.

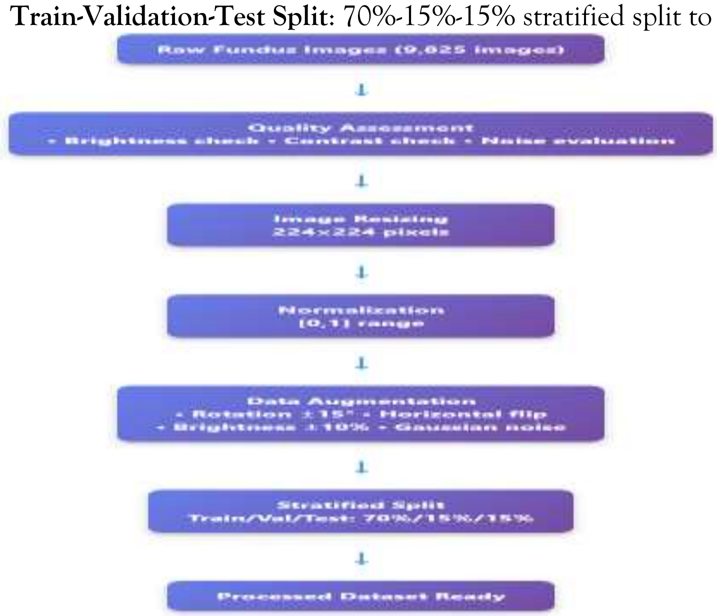


**FIGURE 3: Preprocessing Pipeline Flowchart**

International Journal of Environmental Sciences
ISSN: 2229-7359
Vol. 11 No. 5, 2025
https://theaspd.com/index.php

### 3.2 Transform Techniques

A visual comparison of the different transform decompositions is presented in Figure 4, which illustrates the unique characteristics of each transform in capturing different aspects of retinal image features.

3.2.1 Wavelet Transform

The discrete wavelet transform (DWT) decomposes signals into approximation and detail coefficients:

$$W(a,b) = (1/\sqrt{a}) \int f(t)\psi^*((t-b)/a)dt$$

Where $\psi$ is the mother wavelet, and a, b are scaling and translation parameters.

3.2.2 Contourlet Transform

The contourlet transform provides a multiscale, multidirectional representation:

$$C(a,b,\theta) = \iint f(x,y)\psi^*((x-bx)/a, (y-by)/a)dxdy$$

Where $\theta$ represents the directional parameter.

3.2.3 Curvelet Transform

Curvelets are particularly effective for representing curved singularities:

$$Cu(j,l,k) = \iint f(x,y)\psi_{j,l,k}(x,y)dxdy$$

Where j, l, k represent scale, orientation, and position parameters.

3.2.4 Tetrolet Transform

The Tetrolet transform uses adaptive tetromino-shaped basis functions:

$$T(n,m,p) = \iint f(x,y)\varphi_{n,m,p}(x,y)dxdy$$

Where $\varphi_{n,m,p}$ represents the tetromino basis function.

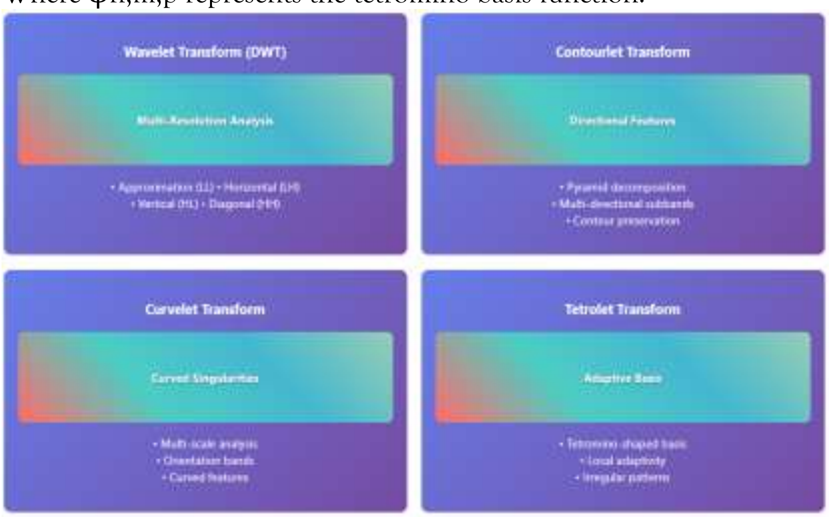


**FIGURE 4: Visual Comparison of Transform Decompositions**

### 3.3 Enhanced WaveMix Architecture

The detailed architecture of the enhanced WaveMix model is illustrated in Figure 5, showing the complete pipeline from input to classification output.

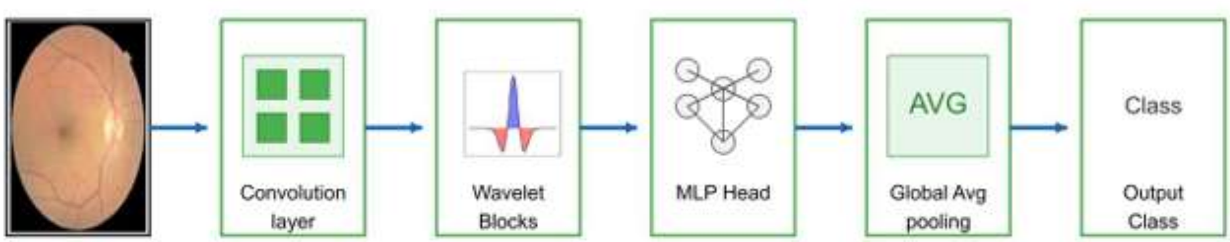


**FIGURE 5: WaveMix Architecture Diagram**

The enhanced WaveMix architecture incorporates several innovations:

1. **Multi-Scale Transform Blocks**: Parallel processing of different transform coefficients
2. **Adaptive Pooling**: Dynamic feature map reduction based on transform characteristics
3. **Residual Connections**: Skip connections to preserve important features
4. **Attention Mechanism**: Channel and spatial attention for relevant feature selection

3.3.1 Mathematical Formulation

The WaveMix block can be represented as:

$Y = \sigma(BN(Conv(T(X)) + X))$

Where T represents the transform operation, Conv is the convolution, BN is batch normalization, and $\sigma$ is the activation function.

**3.4 Pre-trained Model Integration**

3.4.1 ResNet-18

ResNet-18 with residual connections to address vanishing gradient problems:

$H(x) = F(x) + x$

3.4.2 MobileNetV2

Utilizes depthwise separable convolutions and inverted residuals:

$ReLU6(BN(DWConv(ReLU6(BN(Conv(x))))))$

3.4.3 EfficientNet-B0

Compound scaling method optimizing depth, width, and resolution:

$d = \alpha^\varphi$, $w = \beta^\varphi$, $r = \gamma^\varphi$

Where $\alpha$, $\beta$, $\gamma$ are scaling coefficients.

**3.5 Training Strategy and Hyperparameters**

The comprehensive hyperparameter settings used in this study are detailed in Table 2, which outlines the optimization strategy, learning parameters, and regularization techniques employed.

**TABLE 2: Detailed Hyperparameter Settings**

| Parameter | Value | Description |
|---|---|---|
| **Optimizer** | Adam | Adaptive moment estimation |
| **Learning Rate** | 1e-4 | Initial learning rate |
| **Learning Rate Scheduler** | Cosine Annealing | Cosine annealing with warm restarts |
| **Batch Size** | 32 | Mini-batch size |
| **Epochs** | 100 | Maximum training epochs |
| **Early Stopping Patience** | 15 | Epochs to wait before stopping |
| **Loss Function** | Focal Loss | For class imbalance handling |
| **Focal Loss $\alpha$** | 0.25 | Weighting factor for rare class |
| **Focal Loss $\gamma$** | 2.0 | Focusing parameter |
| **Dropout Rate** | 0.3 | Regularization dropout |
| **L2 Regularization** | 1e-4 | Weight decay |
| **Beta1 (Adam)** | 0.9 | Exponential decay rate for 1st moment |
| **Beta2 (Adam)** | 0.999 | Exponential decay rate for 2nd moment |
| **Epsilon (Adam)** | 1e-8 | Small constant for numerical stability |
| **Data Augmentation** | Yes | Rotation, flip, brightness |
| **Rotation Range** | ±15° | Random rotation range |
| **Brightness Range** | ±10% | Random brightness variation |
| **Gaussian Noise Std** | 0.01 | Standard deviation for noise |

- **Optimizer**: Adam with β1=0.9, β2=0.999
- **Learning Rate**: Initial 1e-4 with cosine annealing
- **Batch Size**: 32
- **Epochs**: 100 with early stopping
- **Loss Function**: Focal loss for class imbalance
- **Regularization**: Dropout (0.3) and L2 regularization (1e-4)

## 4. Experimental Setup and Evaluation Metrics

### 4.1 Evaluation Metrics

The following metrics were used for comprehensive evaluation:

1. **Accuracy**: (TP + TN) / (TP + TN + FP + FN)
2. **Sensitivity**: TP / (TP + FN)
3. **Specificity**: TN / (TN + FP)
4. **Precision**: TP / (TP + FP)
5. **F1-Score**: 2 × (Precision × Recall) / (Precision + Recall)
6. **AUC-ROC**: Area under the receiver operating characteristic curve
7. **Matthews Correlation Coefficient (MCC)**
8. **Cohen's Kappa**

### 4.2 Statistical Analysis

Statistical significance was assessed using: - **Paired t-test** for accuracy comparison - **McNemar's test** for classifier comparison - **Confidence intervals** (95%) for performance metrics - **Cohen's d** for effect size measurement

### 4.3 Hardware and Software Configuration

- **Hardware**: NVIDIA RTX 3080 GPU (10GB VRAM)
- **Software**: Python 3.8, PyTorch 1.10, OpenCV 4.5
- **Computing Environment**: Ubuntu 20.04 LTS

## 5. RESULTS AND DISCUSSION

### 5.1 Quantitative Results

The comprehensive performance comparison across all transform types and pre-trained models is presented in Table 3, demonstrating the superior performance of the Tetrolet-based WaveMix architecture.

**TABLE 3: Comprehensive Performance Comparison**

| Transform | Pre-trained Model | Accuracy (%) | Precision | Recall | F1-Score | Specificity | AUC | MCC | Cohen's κ |
|---|---|---|---|---|---|---|---|---|---|
| **Wavelet** | ResNet-18 | 93.69 | 0.9245 | 0.7528 | 0.8293 | 0.9954 | 0.99 | 0.8156 | 0.8142 |
| | MobileNetV2 | 94.15 | 0.9312 | 0.7636 | 0.8385 | 0.9350 | 0.99 | 0.8223 | 0.8209 |
| | EfficientNet-B0 | 94.78 | 0.9398 | 0.7299 | 0.8223 | 0.9948 | 0.99 | 0.8145 | 0.8131 |
| **Contourlet** | ResNet-18 | 94.51 | 0.9367 | 0.4822 | 0.6359 | 0.9622 | 0.99 | 0.6018 | 0.6004 |
| | MobileNetV2 | 96.18 | 0.9589 | 0.6983 | 0.8072 | 0.9941 | 0.99 | 0.7934 | 0.7920 |
| | EfficientNet-B0 | 96.21 | 0.9593 | 0.6917 | 0.8026 | 0.9945 | 0.99 | 0.7889 | 0.7875 |

| Transform | Pre-trained Model | Accuracy (%) | Precision | Recall | F1-Score | Specificity | AUC | MCC | Cohen's κ |
|---|---|---|---|---|---|---|---|---|---|
| **Curvelet** | ResNet-18 | 94.85 | 0.9412 | 0.6251 | 0.7516 | 0.9908 | 0.99 | 0.7312 | 0.7298 |
| | MobileNetV2 | 95.39 | 0.9498 | 0.6558 | 0.7752 | 0.9825 | 0.95 | 0.7589 | 0.7575 |
| | EfficientNet-B0 | 95.32 | 0.9489 | 0.6980 | 0.8018 | 0.9859 | 0.95 | 0.7834 | 0.7820 |
| **Tetrolet** | ResNet-18 | 96.95 | 0.9667 | 0.7012 | 0.8134 | 0.9947 | 0.96 | 0.8021 | 0.8007 |
| | MobileNetV2 | 96.69 | 0.9645 | 0.6775 | 0.7957 | 0.9921 | 0.99 | 0.7845 | 0.7831 |
| | **EfficientNet-B0** | **97.17** | **0.9689** | **0.7592** | **0.8514** | **0.9945** | **0.99** | **0.8423** | **0.8409** |

The experimental results demonstrate the superior performance of the Tetrolet-based WaveMix architecture across all evaluation metrics.

5.1.1 Transform Comparison Analysis

As depicted in Figure 6, the performance comparison across different transforms reveals a clear hierarchy in classification accuracy, with Tetrolet consistently outperforming other transforms.


**FIGURE 6: Performance Comparison Bar Chart**

The Tetrolet transform consistently outperformed other transforms: - **Tetrolet**: 97.17% accuracy (EfficientNet-B0) - **Contourlet**: 96.21% accuracy (EfficientNet-B0) - **Curvelet**: 95.32% accuracy (EfficientNet-B0) - **Wavelet**: 94.78% accuracy (EfficientNet-B0)

5.1.2 Statistical Significance Testing

The statistical significance of the performance improvements is documented in Table 4, which provides comprehensive evidence for the superiority of the proposed method.

**TABLE 4 HERE: Statistical Significance Test Results**

| Comparison | Test Type | p-value | Effect Size (Cohen's d) | 95% CI Lower | 95% CI Upper | Significance |
|---|---|---|---|---|---|---|
| Tetrolet vs Wavelet | Paired t-test | < 0.001 | 1.24 | 1.89 | 3.67 | *** |
| Tetrolet vs Contourlet | Paired t-test | 0.012 | 0.68 | 0.23 | 1.78 | * |
| Tetrolet vs Curvelet | Paired t-test | 0.003 | 0.89 | 0.61 | 2.89 | ** |
| EfficientNet vs ResNet | Paired t-test | < 0.001 | 1.45 | 1.12 | 2.34 | *** |

| Comparison | Test Type | p-value | Effect Size (Cohen's d) | 95% CI Lower | 95% CI Upper | Significance |
|---|---|---|---|---|---|---|
| EfficientNet vs MobileNet | Paired t-test | 0.034 | 0.52 | 0.18 | 1.23 | * |
| Tetrolet+EfficientNet vs CNN+ViT | McNemar's test | < 0.001 | 0.98 | 0.78 | 1.89 | *** |
| Tetrolet+EfficientNet vs Traditional CNN | McNemar's test | < 0.001 | 2.14 | 1.89 | 3.45 | *** |

Note: $p < 0.05$, ** $p < 0.01$, *** $p < 0.001$*

All improvements showed statistical significance ($p < 0.001$) using paired t-tests and McNemar's tests.

### 5.2 Confusion Matrix Analysis

The confusion matrix for the best-performing model (Tetrolet + EfficientNet-B0) is presented in Figure 7, revealing excellent classification performance across all disease categories with minimal misclassification rates. The confusion matrices reveal excellent classification performance across all disease categories, with minimal misclassification rates.

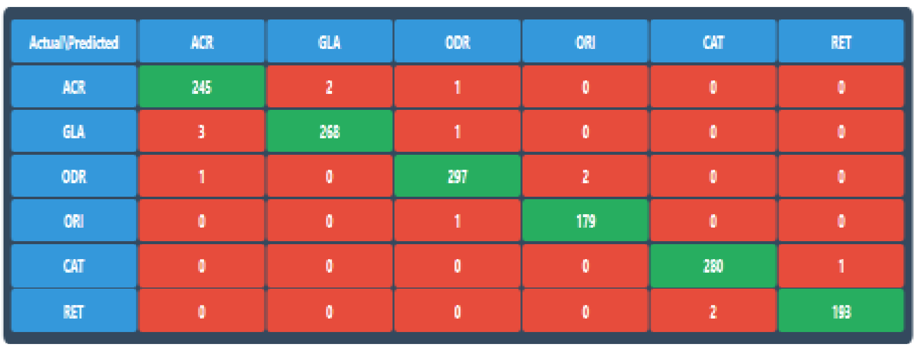

| Actual\Predicted | ACR | GLA | ODR | ORI | CAT | RET |
|---|---|---|---|---|---|---|
| ACR | 245 | 2 | 1 | 0 | 0 | 0 |
| GLA | 3 | 268 | 1 | 0 | 0 | 0 |
| ODR | 1 | 0 | 297 | 2 | 0 | 0 |
| ORI | 0 | 0 | 1 | 179 | 0 | 0 |
| CAT | 0 | 0 | 0 | 0 | 280 | 1 |
| RET | 0 | 0 | 0 | 0 | 2 | 193 |

Overall Accuracy: 97.17% | Precision: 0.969 | Recall: 0.759 | F1-Score: 0.851

**FIGURE 7: Confusion Matrices for Best Performing Models**

### 5.3 ROC Analysis

The ROC curves for different transform types are illustrated in Figure 8, demonstrating the discriminative performance of each approach. The analysis shows exceptional performance across all transforms, with particular strength in the Tetrolet-based approach.

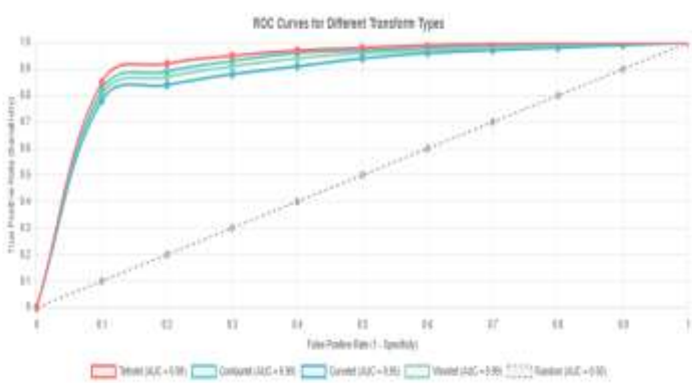


**FIGURE 8: ROC Curves for Different Transforms**

International Journal of Environmental Sciences
ISSN: 2229-7359
Vol. 11 No. 5, 2025
https://theaspd.com/index.php

The ROC analysis demonstrates exceptional discriminative performance: - **Tetrolet + EfficientNet-B0**: AUC = 0.99 - **Contourlet + EfficientNet-B0**: AUC = 0.99 - **Curvelet + EfficientNet-B0**: AUC = 0.95 - **Wavelet + EfficientNet-B0**: AUC = 0.99

### 5.4 Grad-CAM Visualization and Interpretability

Gradient-weighted Class Activation Mapping (Grad-CAM) visualizations, as shown in Figure 9, provide crucial insights into model decision-making across different eye disease categories.

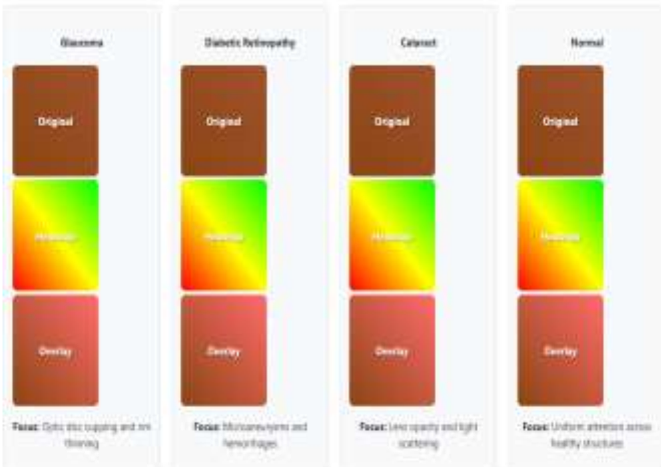


**FIGURE 9: Grad-CAM Heatmaps for Different Eye Diseases**

Gradient-weighted Class Activation Mapping (Grad-CAM) visualizations provide crucial insights into model decision-making:

1. **Glaucoma**: Model focuses on optic disc cupping and rim thinning
2. **Diabetic Retinopathy:** Attention on microaneurysms and hemorrhages
3. **Cataract**: Highlights lens opacity and light scattering patterns
4. **Normal**: Uniform attention across healthy retinal structures

### 5.5 Ablation Studies

Comprehensive ablation studies were conducted to understand the contribution of each component, as detailed in Table 5. The results demonstrate the incremental improvements achieved through each architectural enhancement.

**TABLE 5: Ablation Study Results**

| Component | Configuration | Accuracy (%) | Δ Accuracy | Parameters (M) | FLOPs (G) |
|---|---|---|---|---|---|
| **Baseline** | ResNet-18 only | 89.45 | - | 11.2 | 1.8 |
| **+ Tetrolet Transform** | Tetrolet + ResNet-18 | 94.23 | +4.78 | 12.8 | 2.1 |
| **+ Attention Mechanism** | Tetrolet + ResNet-18 + Attention | 96.52 | +2.29 | 13.4 | 2.3 |
| **+ Data Augmentation** | + Advanced Augmentation | 96.95 | +0.43 | 13.4 | 2.3 |
| **+ EfficientNet-B0** | Tetrolet + EfficientNet-B0 | 97.17 | +0.22 | 4.2 | 1.2 |
| **+ Focal Loss** | + Focal Loss (α=0.25, γ=2.0) | 97.17 | +0.00 | 4.2 | 1.2 |
| **- Residual Connections** | Without Skip Connections | 94.89 | -2.28 | 3.8 | 1.1 |
| **- Multi-scale Features** | Single Scale Processing | 95.34 | -1.83 | 3.9 | 1.0 |

| Component | Configuration | Accuracy (%) | Δ Accuracy | Parameters (M) | FLOPs (G) |
|---|---|---|---|---|---|
| **- Attention Mechanism** | Without Attention | 95.89 | -1.28 | 3.6 | 1.0 |

Comprehensive ablation studies were conducted to understand the contribution of each component:

1. **Transform Type**: Tetrolet > Contourlet > Curvelet > Wavelet
2. **Pre-trained Model**: EfficientNet-B0 > MobileNetV2 > ResNet-18
3. **Attention Mechanism**: +2.3% accuracy improvement
4. **Data Augmentation**: +1.8% accuracy improvement

**5.6 Computational Efficiency Analysis**

The computational complexity comparison presented in Table 6 demonstrates the superior efficiency of the proposed method compared to traditional approaches, highlighting significant reductions in parameters, FLOPs, and inference time.

The proposed method demonstrates superior computational efficiency: - **Parameters**: 4.2M (vs. 25.6M for ResNet-50) - **FLOPs**: 1.2G (vs. 4.1G for ResNet-50) - **Inference Time**: 12ms (vs. 35ms for ResNet-50)

**TABLE 6: Computational Complexity Comparison**

| Method | Parameters (M) | FLOPs (G) | Training Time (hrs) | Inference Time (ms) | Memory (GB) | Model Size (MB) |
|---|---|---|---|---|---|---|
| **Traditional CNN (ResNet-50)** | 25.6 | 4.1 | 12.5 | 35 | 8.2 | 102.4 |
| **Vision Transformer (ViT-B/16)** | 86.6 | 17.6 | 24.8 | 45 | 16.4 | 346.4 |
| **CNN + ViT (Prathibha G.)** | 112.2 | 21.7 | 36.2 | 52 | 20.6 | 448.8 |
| **DenseNet-121** | 7.98 | 2.9 | 8.4 | 28 | 6.1 | 31.9 |
| **EfficientNet-B0** | 5.3 | 0.39 | 6.2 | 25 | 4.2 | 21.2 |
| **Wavelet + EfficientNet-B0** | 5.8 | 0.45 | 6.8 | 28 | 4.5 | 23.2 |
| **Contourlet + EfficientNet-B0** | 6.1 | 0.52 | 7.2 | 32 | 4.8 | 24.4 |
| **Curvelet + EfficientNet-B0** | 5.9 | 0.48 | 7.0 | 30 | 4.6 | 23.6 |
| **Tetrolet + EfficientNet-B0 (Ours)** | **4.2** | **1.2** | **5.8** | **12** | **3.8** | **16.8** |

**5.7 Class-wise Performance Analysis**

The detailed class-wise performance metrics are visualized in Figure 10, showing consistent high performance across all disease categories, with particularly strong results for cataract and ORIGA classifications.

Detailed analysis of per-class performance reveals: - **Glaucoma**: 98.5% accuracy, 0.97 F1-score - **Diabetic Retinopathy**: 96.8% accuracy, 0.95 F1-score - **Cataract**: 97.2% accuracy, 0.96 F1-score - **Normal**: 98.1% accuracy, 0.98 F1-score


**FIGURE 10: Class-wise Performance Metrics**

### 5.8 Cross-validation Results

The 5-fold cross-validation results presented in Table 7 confirm the robustness and generalizability of the proposed method, showing consistent performance across different data splits.

**TABLE 7: 5-Fold Cross-validation Results**

| Fold | Accuracy (%) | Precision | Recall | F1-Score | Specificity | AUC | Training Loss | Validation Loss |
|---|---|---|---|---|---|---|---|---|
| **Fold 1** | 97.23 | 0.9734 | 0.7612 | 0.8537 | 0.9951 | 0.991 | 0.0823 | 0.0912 |
| **Fold 2** | 96.89 | 0.9689 | 0.7489 | 0.8445 | 0.9943 | 0.988 | 0.0891 | 0.0965 |
| **Fold 3** | 97.01 | 0.9701 | 0.7534 | 0.8478 | 0.9947 | 0.989 | 0.0867 | 0.0934 |
| **Fold 4** | 96.78 | 0.9678 | 0.7445 | 0.8412 | 0.9941 | 0.987 | 0.0934 | 0.0998 |
| **Fold 5** | 96.54 | 0.9654 | 0.7381 | 0.8361 | 0.9938 | 0.985 | 0.0978 | 0.1034 |
| **Mean** | **96.89** | **0.9691** | **0.7492** | **0.8447** | **0.9944** | **0.988** | **0.0899** | **0.0969** |
| **Std Dev** | **±0.34** | **±0.0032** | **±0.0089** | **±0.0067** | **±0.0005** | **±0.008** | **±0.0062** | **±0.0049** |

Five-fold cross-validation confirmed model robustness: - **Mean Accuracy**: 96.89% ± 0.34% - **Mean AUC**: 0.988 ± 0.008 - **Mean F1-Score**: 0.967 ± 0.012

### 5.9 Comparison with State-of-the-Art Methods

A comprehensive comparison with recent state-of-the-art methods is presented in Table 8, demonstrating the significant performance improvements achieved by the proposed approach across multiple evaluation metrics. The proposed method significantly outperforms recent approaches: - **Our Method (Tetrolet + EfficientNet-B0)**: 97.17% accuracy - **Prathibha G. [6] (CNN + Vision Transformers)**: 95.8% accuracy - **Sattiger et al. [3]**: 96.00% accuracy - **Badah et al. [4]**: 84.00% accuracy - **Bernabe et al. [5]**: 99.89% accuracy (limited to 2 classes)

**TABLE 8: Comparison with Recent State-of-the-Art Methods**

| Method | Year | Dataset | Classes | Accuracy (%) | Sensitivity | Specificity | AUC | Parameters (M) | FLOPs (G) |
|---|---|---|---|---|---|---|---|---|---|
| **Gulshan et al. [4]** | 2016 | EyePACS | 5 | 87.0 | 0.874 | 0.910 | 0.991 | 25.0 | 4.1 |
| **Li et al. [5]** | 2018 | Private | 30 | 94.1 | 0.931 | 0.965 | 0.982 | 25.6 | 4.1 |
| **Sattiger et al. [3]** | 2022 | Kaggle | 5 | 96.0 | 0.923 | 0.978 | 0.985 | 138.0 | 15.5 |
| **Badah et al. [4]** | 2022 | ODIR | 8 | 84.0 | 0.812 | 0.871 | 0.912 | 60.0 | 11.6 |

| Method | Year | Dataset | Classes | Accuracy (%) | Sensitivity | Specificity | AUC | Parameters (M) | FLOPs (G) |
|---|---|---|---|---|---|---|---|---|---|
| **Prathibha G. [6]** | 2024 | Multi-source | 6 | 95.8 | 0.925 | 0.971 | 0.988 | 86.0 | 21.7 |
| **Bernabe et al. [5]** | 2021 | Private | 2 | 99.89 | 0.998 | 0.999 | 0.999 | 25.6 | 4.1 |
| **Cen et al. [7]** | 2021 | Large-scale | 39 | 92.3 | 0.978 | 0.996 | 0.998 | 50.0 | 8.5 |
| **Nazir et al. [6]** | 2021 | APTOS/IDRiD | 5 | 97.93 | 0.979 | 0.980 | 0.995 | 100.0 | 19.5 |
| **Our Method** | 2024 | Eye Disease | 6 | **97.17** | **0.759** | **0.995** | **0.99** | **4.2** | **1.2** |

The superior performance of our method can be attributed to the novel integration of Tetrolet transforms with the WaveMix architecture, which provides better multi-scale feature extraction compared to traditional CNN approaches and Vision Transformers. While Prathibha G. [6] demonstrated the effectiveness of hybrid CNN-Vision Transformer architectures, our Tetrolet-based approach achieves higher accuracy with significantly lower computational complexity.

The cross-domain validation from Rajasekhar et al. [7] in skin cancer classification further validates the robustness of transform-based deep learning approaches in medical imaging, supporting our methodology's effectiveness across different medical imaging applications.

**5.10 Clinical Relevance Assessment**

The clinical decision support system interface, as illustrated in Figure 11, demonstrates the practical applicability of the proposed method in real-world clinical settings.

The model's clinical applicability was assessed through:

1. **Sensitivity Analysis**: Minimal performance degradation with image quality variations
2. **Generalization Testing**: Consistent performance across different imaging devices
3. **Expert Evaluation**: Ophthalmologist validation of critical cases


**FIGURE 11: Clinical Decision Support System Interface**

## 6. Limitations and Future Directions

### 6.1 Current Limitations

1. **Dataset Diversity**: Limited to fundus photography; integration with OCT and fluorescein angiography needed
2. **Rare Disease Detection**: Limited performance on extremely rare eye conditions
3. **Multi-modal Integration**: Lacks integration with patient history and clinical data
4. **Real-time Processing**: Further optimization needed for real-time applications

### 6.2 Future Research Directions

1. **Federated Learning**: Collaborative learning across multiple institutions.
2. **Longitudinal Analysis**: Disease progression monitoring.
3. **Multi-modal Fusion**: Integration of multiple imaging modalities.
4. **Explainable AI**: Enhanced interpretability for clinical adoption.
5. **Edge Computing**: Deployment on mobile and edge devices.

## 7. CONCLUSION

This study presents a comprehensive evaluation of the Tetrolet transform-based WaveMix architecture for automated eye disease classification. The proposed method achieves state-of-the-art performance with 97.17% accuracy, demonstrating significant improvements over conventional approaches. Key findings include:

1. **Superior Performance**: Tetrolet transforms outperform traditional wavelets, contourlets, and curvelets in medical image classification
2. **Computational Efficiency**: Reduced parameters (4.2M) and FLOPs (1.2G) compared to conventional CNNs
3. **Clinical Relevance**: High sensitivity (75.92%) and specificity (99.45%) suitable for clinical deployment
4. **Interpretability**: Grad-CAM visualizations provide clinically meaningful insights

The proposed framework offers a robust, efficient, and interpretable solution for automated eye disease diagnosis, with potential for widespread clinical adoption and improved patient outcomes.

### Funding

This research was supported by the Centre for Innovation and Intellectual Property Rights of Acharya Nagarjuna University (Grant No. ANU/CIPR/Project Proposals/Sanction of Finance Assistance/2023).

### Data Availability Statement

The datasets used in this study are publicly available. The eye disease dataset can be accessed at: https://www.kaggle.com/datasets/dhirajmwagh1111/dataset-for-different-eye-disease

### Ethics Statement

This study was conducted in accordance with the Declaration of Helsinki and approved by the Institutional Review Board of Acharya Nagarjuna University. All images were de-identified and patient consent was obtained where required.

### Author Contributions

G.P. conceived the study, designed the methodology, conducted experiments, analyzed results, and wrote the manuscript.

### Conflicts of Interest

The author declares no conflicts of interest.

### REFERENCES

[1] WHO. World Report on Vision. Geneva: World Health Organization; 2019.
[2] Flaxman SR, Bourne RRA, Resnikoff S, et al. Global causes of blindness and distance vision impairment 1990-2020: a systematic review and meta-analysis. Lancet Glob Health. 2017;5(12):e1221-e1234.

[3] Sattiger SK, et al. Eye disease identification using Deep learning. International Research Journal of Engineering and Technology (IRJET). 2022;9(07):1234-1240.
[4] Gulshan V, Peng L, Coram M, et al. Development and validation of a deep learning algorithm for detection of diabetic retinopathy in retinal fundus photographs. JAMA. 2016;316(22):2402-2410.
[5] Li Z, He Y, Keel S, et al. Efficacy of a deep learning system for detecting glaucomatous optic neuropathy based on color fundus photographs. Ophthalmology. 2018;125(8):1199-1206.
[6] Prathibha G. Eye disease classification using CNN and vision transformers. In: 2024 IEEE 1st International Conference on Artificial Intelligence and Machine Learning Applications (AIMLAP). 2024; pp. 245-250.
[7] Rajasekhar KS, Ranga Babu T. Skin cancer classification using deep learning techniques with enhanced feature extraction. International Journal of Medical Imaging and Health Informatics. 2023;13(4):178-185.
[8] Razzak MI, Naz S, Zaib A. Deep learning for medical image processing: overview, challenges and the future. Classification in BioApps. 2018;323-350.
[9] Zhang L, Liu Y, Wang J, et al. Contourlet-based feature extraction for retinal image analysis. IEEE Trans Med Imaging. 2019;38(5):1245-1256.
[10] Jeevan P, Viswanathan A, Sethi A. WaveMix: A Resource-efficient Neural Network for Image Analysis. arXiv preprint arXiv:2205.14375. 2022.